

This work was written as part of one of the author's official duties as an Employee of the United States Government and is therefore a work of the United States Government. In accordance with 17 U.S.C. 105, no copyright protection is available for such works under U.S. Law.

Public Domain Mark 1.0

<https://creativecommons.org/publicdomain/mark/1.0/>

Access to this work was provided by the University of Maryland, Baltimore County (UMBC) ScholarWorks@UMBC digital repository on the Maryland Shared Open Access (MD-SOAR) platform.

Please provide feedback

Please support the ScholarWorks@UMBC repository by emailing scholarworks-group@umbc.edu and telling us what having access to this work means to you and why it's important to you. Thank you.

Using Shape to Control Photoluminescence from CdSe/CdS Core/Shell Nanorods

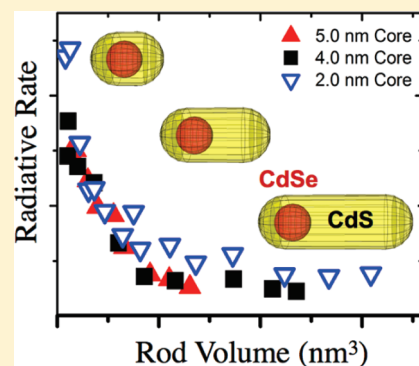
Chunxing She, Arnaud Demortière, Elena V. Shevchenko, and Matthew Pelton*

Center for Nanoscale Materials, Argonne National Laboratory, 9700 South Cass Avenue, Argonne, Illinois 60439, United States

S Supporting Information

ABSTRACT: CdSe/CdS core/shell nanorods can exhibit high photoluminescence quantum yields, but it is not yet clear what processes determine the yields and how they can be controlled. Moreover, the effective band alignment between the core and the shell affects quantum yield, but its nature is still under debate. We systematically studied quantum yields when the shell is excited as a function of both core size and shell volume. Using time-resolved photoluminescence decay measurements and transient-absorption spectroscopy, we found that quantum yields are determined by a balance between radiative and nonradiative recombination rates, and not by single-carrier trapping. The radiative recombination rate decreases as the nanorod volume increases, independent of the core size. The results indicate that high quantum yields can be obtained only by limiting the size of the shell and point to an effective quasi-type-II band alignment for all of the nanorods in this study.

SECTION: Nanoparticles and Nanostructures



Semiconductor nanocrystals are promising materials for a wide range of technologies, including light-emitting devices,^{1–3} lasing media,^{4–7} luminescent solar concentrators,^{8–10} and biological labels,^{11–14} due to their high photostability and their potential for high luminescence quantum yields (QYs). Nanocrystal QYs are determined by the balance between radiative and nonradiative processes and can thus be increased by minimizing nonradiative pathways such as charge trapping. This has been realized by coating nanocrystal surfaces with organic molecules or inorganic shells, thus limiting the number of uncoordinated atoms at the surfaces.^{15,16}

Rod-shaped CdSe/CdS core/shell heterostructures,^{4,17–29} in particular, have been observed to exhibit high photoluminescence (PL) QYs (up to 80% when exciting the core).^{20,24} These structures are also of interest due to the ability to tune the energy difference (known as the quasi-Stokes shift) between their optical absorption and emission maxima. Large quasi-Stokes shifts minimize reabsorption of emitted light in materials containing these nanorods (NRs), improving their performance in devices such as scintillation detectors and luminescent solar concentrators. For these applications, light is absorbed predominantly by the large CdS shell, so that the most relevant property of the NRs is the QY for luminescence from the CdSe core following excitation of the CdS shell. If excitation of the shell is followed by rapid electron or hole trapping by surface or defect states, low QY will result. Even if trapping is avoided, high QY still requires that radiative recombination be fast compared to nonradiative recombination. Previous results on NRs with biexponential PL decays indicated that the decay time increases with the aspect ratio of the NRs,²⁴ but a more complete

understanding of radiative and nonradiative recombination rates has so far been lacking.

One important factor in determining recombination rates is the spatial extent of the carriers, that is, whether the electrons and holes are localized within the CdSe core or are delocalized throughout the nanorods. It is generally accepted that the lowest-energy hole states are confined to the core because the valence-band-edge energy is significantly higher in CdSe than that in CdS. On the other hand, there is a debate in the literature with regard to whether the lowest-energy electrons are also localized in the core, reflecting what is known as type-I band alignment, or whether they are delocalized throughout the NRs, known as quasi-type-II band alignment. Direct measurements of conduction band offsets using scanning tunneling microscopy indicated a difference of 0.3 eV, leading to the conclusion of type-I band offset in the rods studied.¹⁸ Multiexciton spectroscopy suggested a transition from type-I electron localization to quasi-type-II electron delocalization when the CdSe core is smaller than 2.8 nm in diameter.¹⁹ Exciton localization was also directly imaged using near-field techniques.³⁰ However, numerous optical measurements^{17,20,22–24,26} and electronic structure calculations²⁷ support quasi-type-II band offsets for CdSe/CdS core/shell nanorods. The success of photocatalytic hydrogen production using CdSe/CdS nanorods with Pt tips also strongly suggests that electrons are delocalized in the CdS shells before being transferred to the Pt tips.²⁹

Received: April 14, 2011

Accepted: May 19, 2011

Published: June 01, 2011

In an effort to gain control over QYs of CdSe/CdS NRs and to gain a better understanding of the type of electron localization/delocalization present in these NRs, we study QYs and photo-physical processes by systematically (1) tuning the shell size while keeping the core size fixed and (2) changing the core size in the range from 2.0 to 5.0 nm. No significant trapping of electrons or holes is observed (as opposed to trap-mediated electron–hole recombination), regardless of nanoparticle volume. Radiative decay rates can be quantitatively correlated with the rod volume, regardless the size of the core, indicating that all of the nanorods studied exhibit effective quasi-type-II band alignment. The nanorod volume is thus the main factor controlling QY, and high yields can be obtained only for relatively small CdS shells.

We first measure PL QYs of CdSe/CdS NRs for different volumes of CdSe cores and CdS shells. NRs with core sizes of 2.0,

4.0, and 5.0 nm are synthesized following a modification of the seeded-growth procedure previously reported (see Supporting Information).^{20,24} The larger cores are prolate spheroids; in this case, we use “core size” to refer to the larger of their two diameters. In previous measurements, high QYs were obtained by exciting the higher-energy transition of the CdSe core^{20,22} or somewhere below the band gap transition of CdS.^{24,31} By contrast, we measure QYs by exciting the shell at 2.76 eV (450 nm), obtaining values that are more relevant for applications such as luminescent solar concentrators. We note that the absorption at this photon energy by the CdS shells is between 5 and 50 times larger than the absorption by the CdSe cores (see below), so that we neglect direct absorption into CdSe. As shown in Figure 1, increasing the size of the rod results in lower QY.^{22,24} Here, rod size is described in terms of the total volume of the core/shell particle because we found that this volume uniquely dictates radiative recombination rates (see below). For NRs with a core size of 2.0 nm, the QY decreases relatively slowly with the rod volume, as compared to NRs with 4.0 and 5.0 nm cores.

To determine the mechanisms responsible for these size-dependent QYs and for the differences between NRs with different core sizes, we examined the steady-state and time-resolved optical absorption and emission properties of the NRs. Figure 2 illustrates the steady-state properties for CdSe/CdS core/shell NRs with 2.0 nm CdSe cores. Corresponding data for NRs with 4.0 and 5.0 nm cores show the same trends (see the Supporting Information). In order to correlate the optical properties to the nanoparticle structures, we measured the NR dimensions from TEM images, such as the ones shown in Figures 2a–d. Full information about the NR dimensions for all of the measured samples is given in Table S1 (Supporting

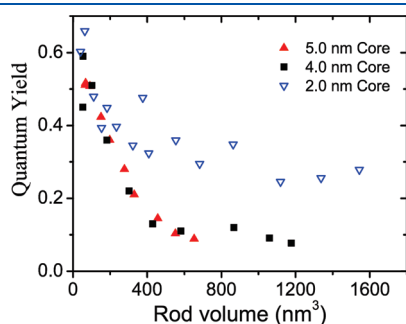


Figure 1. QYs as a function of nanorod volume for CdSe/CdS core/shell nanorods with different core sizes (2.0, 4.0, and 5.0 nm), obtained by exciting the shell with a photon energy of 2.76 eV (450 nm).

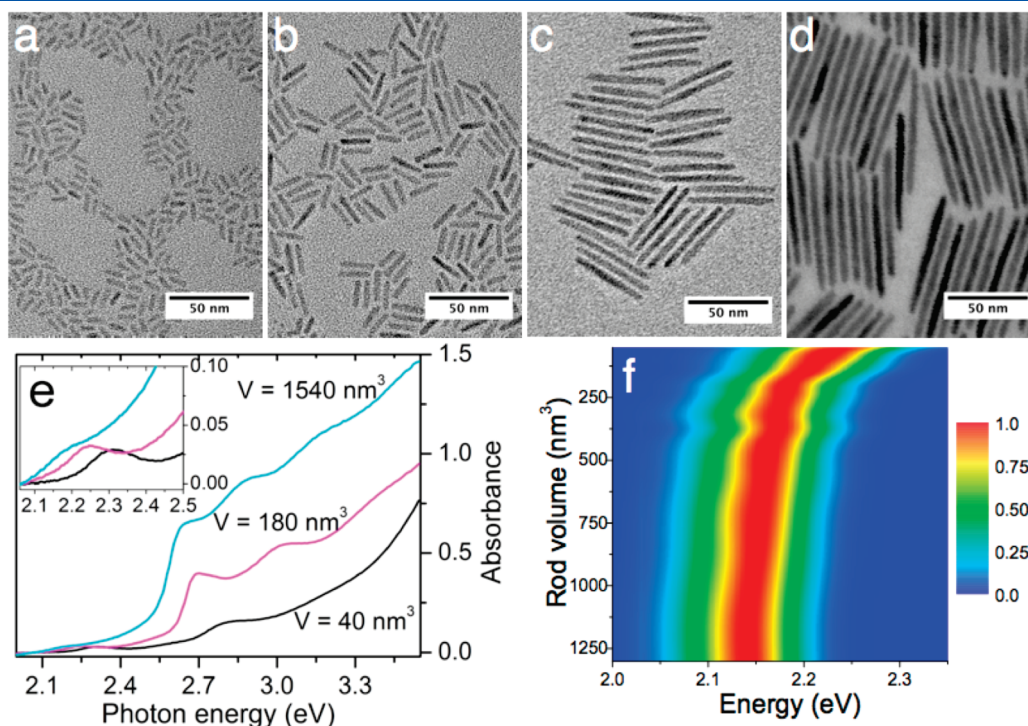


Figure 2. Properties of CdSe/CdS core/shell nanorods with 2.0 nm CdSe cores. (a–d) Transmission electron microscope images showing nanorods with lengths of 9, 18, 41, and 70 nm, corresponding to rod volumes, V , of 60, 180, 500, and 1540 nm³, respectively. (e) Optical absorption spectra for nanorods with different volumes. The inset shows a magnified view of the absorption in the energy region from 2.1 to 2.5 eV. (f) Contour plot of emission spectra for nanorods with different rod volumes; the color scale represents normalized emission intensity.

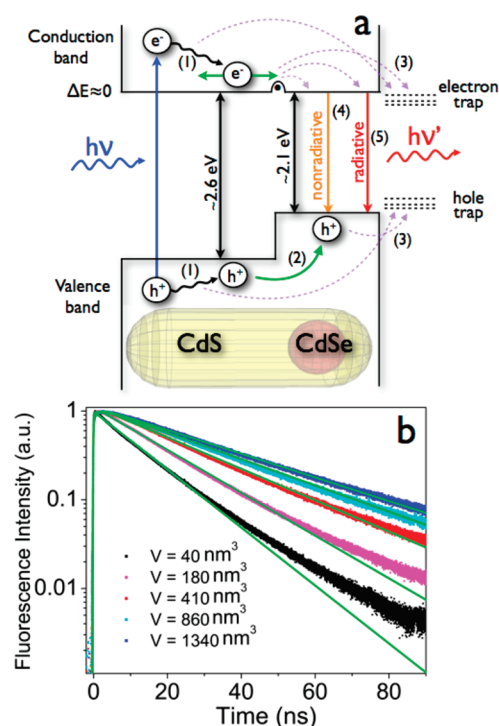


Figure 3. (a) Sketch of the proposed quasi-type-II band alignment in CdSe/CdS core/shell nanorods and possible processes following above-band optical excitation: (1) carrier relaxation, (2) hole transfer to the CdSe core, (3) carrier trapping, (4) nonradiative recombination, and (5) radiative recombination. Effective CdS and CdSe band gap energies depend on the nanorod dimensions; the values given are representative. (b) Photoluminescence decays for CdSe/CdS core/shell nanorods with 2.0 nm cores and different rod volumes, V . The green solid lines are exponential fits to the decays, shown in order to illustrate the small deviation of the measured data from single-exponential decay.

Information), and distributions of NR volumes are illustrated in Figure S2 (Supporting Information). Figure 2e shows absorption spectra for three particular NR samples; the peaks at approximately 2.7 and 2.2 eV are the 1S transitions of CdS and CdSe, respectively. As expected, NRs with larger volumes show more dominant absorption of CdS for photon energies above 2.7 eV. Figure 2f shows a contour plot of emission spectra for NRs with different rod volumes. The emission peak at approximately 2.15 eV comes purely from the CdSe cores.^{20,22}

Both the absorption and emission spectra show a progressive decrease of the CdSe transition energy with increasing rod volume. This red shift is typical for a carrier that is delocalized across the entire nanorod, reflecting a decrease in the quantum confinement energy.^{32,33} Similar results are obtained for NRs with 4.0 and 5.0 nm cores (Figures S3 and S4, Supporting Information), indicating that all NRs examined herein have similar carrier delocalization.

The absorption and emission spectra (Figure 2e,f) therefore indicate that the electron or hole or both are delocalized throughout the NRs. The valence band offset between CdSe and CdS is known to be large though, meaning that the ground-state hole wave function must be localized in the CdSe core. By contrast, the effective conduction band offset is small or 0, so that the electron wave function can extend into both materials. In other words, the absorption and emission spectra suggest a quasi-type-II band structure of the NRs, as shown in Figure 3a.

Also shown are the various processes that can follow photoexcitation of an electron–hole pair above the CdS band gap energy.^{26,34–37} In order from fastest to slowest, they are (1) electron and hole relaxation to the band edges, (2) hole transfer to the core, (3) trapping of an electron or hole, meaning transfer of a single carrier to a localized state that quenches luminescence, with the other carrier remaining in its original state, (4) nonradiative recombination of band-edge carriers, and (5) radiative recombination of band-edge carriers. Processes (3) and (4) can result in loss of the PL QY. We note that we use the term “trapping” to refer exclusively to transfer of a single carrier from a conduction band or valence band state to a trap state; trap-mediated processes that result in the annihilation of an electron–hole pair, by contrast, are included in the category of nonradiative recombination. We perform all of our experiments in the low-excitation limit, where at most one electron–hole pair at a time is created within the nanocrystal, so that Auger decay and other multiexciton processes can be neglected (see details in the Supporting Information).

In order to gain insight into the single-exciton processes, we measured PL decay dynamics, exciting the samples with a frequency-doubled Ti:Sapphire laser (excitation energy of 3.1 eV) and using a time-correlated single-photon counting apparatus for time-resolved detection of emission. Figure 3b shows the PL decay dynamics for CdSe/CdS NRs with 2.0 nm cores; corresponding data for 4.0 and 5.0 nm cores are given in the Supporting Information (Figure S5). The PL decay rate gradually decreases as the nanorod volume increases. For all of the samples measured, over 90% of the PL decay can be described by a single exponential. Carrier trapping is expected to lead to multiexponential decay, with a fast decay component corresponding to the trapping rate; this has been observed, for example, when electron- or hole-trapping molecules have been deliberately adsorbed onto nanocrystal surfaces.^{38–40} We can thus conclude that carrier trapping in these core/shell nanorods is negligible, so that nearly every photoexcited electron–hole pair relaxes to the band-edge state and then recombines either radiatively or nonradiatively. We note that the deviation from single exponential is greatest for the smallest rods; if surface trapping were responsible for nonexponential decay, it would be expected to be more significant for the larger rods, which have larger surface areas. We note also that closely related “giant” nanocrystals with CdSe cores and thick, spherical CdS cores have been shown to have strongly suppressed blinking behavior, consistent with the lack of surface trapping in these systems.^{41,42} These nanocrystals have also been observed to exhibit single-exponential PL whose decay rate decreases with increasing shell thickness.⁴³ The measured PL lifetimes are more sensitive to the amount of CdS shell material in the spherical nanoparticles, pointing to the importance of shape in determining the emission properties of these core/shell nanoparticles.

In addition, the nearly single-exponential photoluminescence decay suggests a relatively homogeneous distribution of decay rates in each nanorod sample. Given the homogeneity in both the decay rates and rod shapes as shown by TEM (Figure 2a–d), the measured ensemble-averaged QY and PL decay time represent approximately the parameters of each individual nanorod.⁴⁴

With these two conclusions — that there is no significant carrier trapping and that the measured ensemble photoluminescence decay is representative of all of the individual NRs in the ensemble — it is straightforward to calculate radiative and

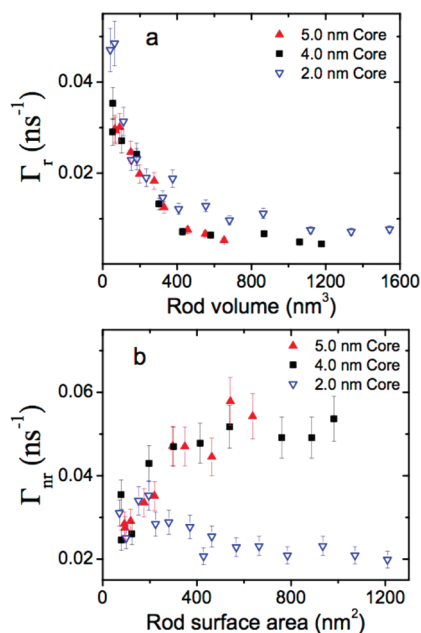


Figure 4. (a) Radiative decay rates, Γ_r , as a function of nanorod volume for CdSe/CdS core/shell nanorods with different sizes of CdSe cores. (b) Nonradiative decay rates, Γ_{nr} , as a function of nanorod surface area for the same nanorod samples. Radiative and nonradiative rates are determined from measured QYs and photoluminescence lifetimes using eq 1.

nonradiative decay rates, Γ_r and Γ_{nr} , based on the measured QYs and PL lifetimes:

$$\eta = \frac{\Gamma_r}{\Gamma_r + \Gamma_{nr}} = \Gamma_r \cdot \tau_o \quad (1)$$

where η is the PL QY and τ_o is the observed PL lifetime.⁴⁵ We use the $1/e$ decay time to approximate τ_o (i.e., the time at which the PL signal has decayed from its maximum value by a factor of e); full results are given in Table S1 (Supporting Information). Figure 4a shows the radiative decay rates determined in this way as a function of NR volume. The radiative decay rate decreases as the volume increases, following the same universal trend regardless of the different core sizes (2.0, 4.0, and 5.0 nm). Plots of radiative decay rates versus aspect ratios or lengths of NRs do not yield the same universal scaling (see Figure S6, Supporting Information). The observed scaling of the radiative decay rate with nanorod volume is evidence that the overlap between the electron and hole wave functions decreases as the rod volume increases,¹⁷ indicating that the electron is delocalized throughout the entire NR. In other words, the universal behavior is compelling evidence for the quasi-type-II character of those core/shell heterostructures, regardless of core size. This scaling is also consistent with a simple calculation of electron–hole overlaps for spherical core–shell systems.⁴⁶ Although the dependence of radiative decay rate on volume is nearly identical for all of the samples studied, there is a small difference at larger volumes between the samples with 4.0 and 5.0 nm cores and the samples with 2.0 nm cores. This deviation is most likely due to the greater heterogeneity of the samples with larger cores, resulting in slightly nonexponential decays and thus less accurate determination of radiative rates from exponential fits (see Figure S5 in the Supporting Information).

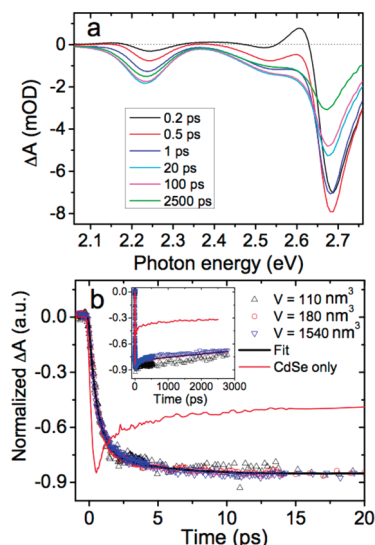


Figure 5. (a) Transient absorption spectra of CdSe/CdS core/shell nanorods with 2.0 nm cores and 180 nm^3 volumes, following excitation with a photon energy of 3.10 eV (400 nm). (b) Transient absorption kinetics for CdSe/CdS core/shell nanorods with 2.0 nm cores and different volumes. The inset shows the same data over a longer time range. The probe energies are 2.26, 2.22, and 2.17 eV for nanorod volumes of 110, 180, and 1540 nm^3 , respectively, all of which correspond to the CdSe bleach minima. Also shown are the kinetics for bare CdSe nanoparticles, with no CdS shell.

Figure 4b shows the nonradiative decay rate as a function of the surface area of the rods; in this case, we choose surface area rather than volume as the relevant geometrical parameter because it should be proportional to the number of surface defects. The nonradiative decay rates for NRs with 2.0 nm CdSe cores depend only weakly on the surface area. For NRs with 4.0 and 5.0 nm cores, by contrast, the nonradiative decay rates increase dramatically with the rod surface area. The additional nonradiative pathways that are present in the NRs with larger cores may be related to surface states, to defects in the bulk of the semiconductor, or to strain-induced defects at the CdSe/CdS interface.^{47–49}

Our main conclusions — quasi-type-II band alignment and the absence of significant electron or hole trapping in the NRs — are also supported by transient absorption (TA) spectroscopy. We again illustrate the properties of all of the samples with data from CdSe/CdS NRs with 2.0 nm cores. Figure 5a shows the transient absorption spectra for NRs with an average volume of 180 nm^3 , following excitation of the CdS shell at 3.10 eV (400 nm). The CdS bleach signal at approximately 2.68 eV reaches its maximum within 0.5 ps due to carrier relaxation and state filling.^{50,51} Similar behavior can be seen in the transient spectra and bleach dynamics of pure CdS NRs under the same experimental conditions (Figures S7 and S8, Supporting Information). Because the state-filling-induced bleach signal is dominated by the electron,^{50,52} the similarity suggests similar transient electron dynamics and delocalization in CdSe/CdS and CdS NRs. Further evidence that the bleach signal at 2.68 eV for the CdSe/CdS core/shell nanorods comes from the CdS shell is provided by the 2:1 ratio of this signal at 2500 ps to the CdSe 1S bleach signal at 2.25 eV; if the signal came from the 1P transition of CdSe, it would be much smaller than the CdSe 1S transition, as observed for pure CdSe nanocrystals (see Figure S7, Supporting

Information). The large bleach at 2.68 eV is thus direct evidence of state filling in CdS, and its large value at 2500 ps is evidence that the electron remains delocalized in the shell well after the initial excitation. This provides further support for the quasi-type-II character of these heterostructures.²⁶

Unlike the ultrafast growth of the CdS bleach, the bleach of the CdSe 1S transition at 2.25 eV grows relatively slowly, reaching its maximum in 10–20 ps. This slow growth of the CdSe bleach is distinctly different from the fast growth in pure CdSe QDs, which occurs in less than 0.5 ps and is due to relaxation of high-energy carriers (Figure S5b and S7, Supporting Information). The relatively slow growth in CdSe/CdS core/shell NRs is attributed to hole transfer from CdS to CdSe (process (2) in Figure 3a).²⁶ Figure 5b shows the dynamics of hole transfer for NRs with different volumes but the same 2.0 nm CdSe core. The hole-transfer dynamics appears to be independent of rod volume from approximately 100 to 1500 nm³. The dynamics can be fit with two exponentials with time constants of 0.62 ± 0.02 and 4.5 ± 0.3 ps, consistent with previously reported hole-transfer rates;²⁶ similar results are obtained for NRs with 4.0 or 5.0 nm cores (Figure S9, Supporting Information). The fact that the measured time constants are independent of shell size indicates that there are no size-dependent hole-trapping processes that compete with hole transfer. The time constants can be compared to those for carrier transfer in true type-II nanocrystal heterostructures, such as ZnSe/CdS “nanobarbells” consisting of CdS nanorods with ZnSe tips.⁵³ In these structures, transfer of photoexcited electrons from ZnSe to CdS is fast, occurring in less than 1 ps, whereas hole transfer from CdS to ZnSe is much slower, taking about 100 ps. The rate of hole transfer from CdS to CdSe in our core/shell nanorods is intermediate between these values, reflecting the different driving energies for the carrier-transfer processes and the different geometry of the heterostructures.

The inset in Figure 5b shows decay dynamics for the CdSe 1S exciton after hole transfer. For pure CdSe nanoparticles, the signal rapidly decays to less than half of its initial value due to carrier trapping; by contrast, in CdSe/CdS NRs, the signal shows no rapid decay and is only about 15% less than its maximum value even after 2500 ps. This indicates that there is no significant carrier trapping in the CdSe/CdS core/shell NRs on nanosecond time scales, consistent with the PL decay measurements. This further validates the use of eq 1 to estimate radiative and nonradiative decay rates.

The observation that radiative decay rates are dictated by rod volumes provides strong evidence for quasi-type-II effective band alignment in all of the NR structures that we studied, which is further supported by the steady-state emission spectra and transient absorption data. We note that a very recent report comes to the same conclusion of electron delocalization using temperature-dependent photoluminescence lifetime measurements, for core sizes from 2.2 to 3.3 nm.⁵⁴ On the other hand, previous studies have reported type-I band offsets in at least some CdSe/CdS core/shell nanorods.^{18,19,30} The discrepancy could be due to subtle differences in the shape of the nanoparticles, which have been reported to dramatically affect the effective band offsets.²⁸ Structural differences at the CdSe/CdS interface, such as strain and alloying, may also change the effective band alignments.

In summary, we investigated the photophysical properties of CdSe/CdS NRs and related them to photoluminescence QY. Transient absorption and time-resolved luminescence measurements

indicate no significant trapping of electrons or holes. The hole is localized into the core within 10 ps, with a transfer rate that is independent of the size of the shell, and the electron remains delocalized in the shell. Radiative decay rates can be quantitatively correlated with the rod volume regardless of the size of the CdSe core for core sizes in the measured range from 2.0 to 5.0 nm. A more quantitative understanding of how the radiative recombination rate depends on nanoparticle geometry requires a detailed theoretical model, which is currently in progress. The other main question to be resolved in future work is the microscopic mechanism responsible for nonradiative recombination in these nanoparticles. Nonetheless, the understanding gained in the current work allows us to say that QYs of CdSe/CdS core/shell NRs can be optimized by maximizing radiative decay rates, which, in turn, requires relatively small rod volumes. In principle, this understanding should apply to all type-II heterostructure nanoparticles.

■ ASSOCIATED CONTENT

S Supporting Information. Details of synthesis of semiconductor nanoparticles, optical measurements, and nanorod properties. This material is available free of charge via the Internet at <http://pubs.acs.org>.

■ AUTHOR INFORMATION

Corresponding Author

*Tel: 630-252-4598. Fax: 630-252-4646. E-mail: pelton@anl.gov.

■ ACKNOWLEDGMENT

Work at the Center for Nanoscale Materials was supported by the U.S. Department of Energy, Office of Science, Office of Basic Energy Sciences, under Contract No. DE-AC0206CH-11357. We thank Seth Darling, Jeffrey Guest, Tijana Rajh, Gary Wiederrecht, and Richard Schaller for helpful discussions, David Gosztola for help with pump–probe measurements, and David Potterveld and Roy Holt for their input and for initiating the project that led to this work.

■ REFERENCES

- (1) Zhao, J. L.; Bardecker, J. A.; Munro, A. M.; Liu, M. S.; Niu, Y. H.; Ding, I. K.; Luo, J. D.; Chen, B. Q.; Jen, A. K. Y.; Ginger, D. S. Efficient CdSe/CdS Quantum Dot Light-Emitting Diodes Using a Thermally Polymerized Hole Transport Layer. *Nano Lett.* **2006**, *6*, 463–467.
- (2) Coe, S.; Woo, W. K.; Bawendi, M.; Bulovic, V. Electroluminescence from Single Monolayers of Nanocrystals in Molecular Organic Devices. *Nature* **2002**, *420*, 800–803.
- (3) Anikeeva, P. O.; Halpert, J. E.; Bawendi, M. G.; Bulovic, V. Quantum Dot Light-Emitting Devices with Electroluminescence Tunable over the Entire Visible Spectrum. *Nano Lett.* **2009**, *9*, 2532–2536.
- (4) Kazes, M.; Lewis, D. Y.; Ebenstein, Y.; Mokari, T.; Banin, U. Lasing from Semiconductor Quantum Rods in a Cylindrical Microcavity. *Adv. Mater.* **2002**, *14*, 317–321.
- (5) Klimov, V. I.; Ivanov, S. A.; Nanda, J.; Achermann, M.; Bezel, I.; McGuire, J. A.; Piryatinski, A. Single-Exciton Optical Gain in Semiconductor Nanocrystals. *Nature* **2007**, *447*, 441–446.
- (6) Zavelani-Rossi, M.; Lupo, M. G.; Krahne, R.; Manna, L.; Lanzani, G. Lasing in Self-Assembled Microcavities of CdSe/CdS Core/Shell Colloidal Quantum Rods. *Nanoscale* **2010**, *2*, 931–935.
- (7) Garcia-Santamaria, F.; Chen, Y. F.; Vela, J.; Schaller, R. D.; Hollingsworth, J. A.; Klimov, V. I. Suppressed Auger Recombination In

"Giant" Nanocrystals Boosts Optical Gain Performance. *Nano Lett.* **2009**, *9*, 3482–3488.

(8) Currie, M. J.; Mapel, J. K.; Heidel, T. D.; Goffri, S.; Baldo, M. A. High-Efficiency Organic Solar Concentrators for Photovoltaics. *Science* **2008**, *321*, 226–228.

(9) Barnham, K.; Marques, J. L.; Hassard, J.; O'Brien, P. Quantum-Dot Concentrator and Thermodynamic Model for the Global Redshift. *Appl. Phys. Lett.* **2000**, *76*, 1197–1199.

(10) Sholin, V.; Olson, J. D.; Carter, S. A. Semiconducting Polymers and Quantum Dots in Luminescent Solar Concentrators for Solar Energy Harvesting. *J. Appl. Phys.* **2007**, *101*, 123114.

(11) Alivisatos, P. The Use of Nanocrystals in Biological Detection. *Nat. Biotechnol.* **2004**, *22*, 47–52.

(12) Hahn, M. A.; Tabb, J. S.; Krauss, T. D. Detection of Single Bacterial Pathogens with Semiconductor Quantum Dots. *Anal. Chem.* **2005**, *77*, 4861–4869.

(13) Ruan, G.; Agrawal, A.; Marcus, A. I.; Nie, S. Imaging and Tracking of Tat Peptide-Conjugated Quantum Dots in Living Cells: New Insights into Nanoparticle Uptake, Intracellular Transport, and Vesicle Shedding. *J. Am. Chem. Soc.* **2007**, *129*, 14759–14766.

(14) Michalet, X.; Pinaud, F. F.; Bentolila, L. A.; Tsay, J. M.; Doose, S.; Li, J. J.; Sundaresan, G.; Wu, A. M.; Gambhir, S. S.; Weiss, S. Quantum Dots for Live Cells, In Vivo Imaging, and Diagnostics. *Science* **2005**, *307*, 538–544.

(15) Qu, L. H.; Peng, X. G. Control of Photoluminescence Properties of CdSe Nanocrystals in Growth. *J. Am. Chem. Soc.* **2002**, *124*, 2049–2055.

(16) Hines, M. A.; Guyot-Sionnest, P. Synthesis and Characterization of Strongly Luminescing ZnS-Capped CdSe Nanocrystals. *J. Phys. Chem.* **1996**, *100*, 468–471.

(17) Muller, J.; Lupton, J. M.; Lagoudakis, P. G.; Schindler, F.; Koeppe, R.; Rogach, A. L.; Feldmann, J.; Talapin, D. V.; Weller, H. Wave Function Engineering in Elongated Semiconductor Nanocrystals with Heterogeneous Carrier Confinement. *Nano Lett.* **2005**, *5*, 2044–2049.

(18) Steiner, D.; Dorfs, D.; Banin, U.; Della Sala, F.; Manna, L.; Millo, O. Determination of Band Offsets in Heterostructured Colloidal Nanorods Using Scanning Tunneling Spectroscopy. *Nano Lett.* **2008**, *8*, 2954–2958.

(19) Sitt, A.; Della Sala, F.; Menagen, G.; Banin, U. Multiexciton Engineering in Seeded Core/Shell Nanorods: Transfer from Type-I to Quasi-Type-II Regimes. *Nano Lett.* **2009**, *9*, 3470–3476.

(20) Talapin, D. V.; Nelson, J. H.; Shevchenko, E. V.; Aloni, S.; Sadtler, B.; Alivisatos, A. P. Seeded Growth of Highly Luminescent CdSe/CdS Nanoheterostructures with Rod and Tetrapod Morphologies. *Nano Lett.* **2007**, *7*, 2951–2959.

(21) Becker, K.; Lupton, J. M.; Muller, J.; Rogach, A. L.; Talapin, D. V.; Weller, H.; Feldmann, J. Electrical Control of Forster Energy Transfer. *Nat. Mater.* **2006**, *5*, 777–781.

(22) Talapin, D. V.; Koeppe, R.; Gotzinger, S.; Kornowski, A.; Lupton, J. M.; Rogach, A. L.; Benson, O.; Feldmann, J.; Weller, H. Highly Emissive Colloidal CdSe/CdS Heterostructures of Mixed Dimensionality. *Nano Lett.* **2003**, *3*, 1677–1681.

(23) Saba, M.; Minniberger, S.; Quochi, F.; Roither, J.; Marceddu, M.; Gocalinska, A.; Kovalenko, M. V.; Talapin, D. V.; Heiss, W.; Mura, A.; et al. Exciton–Exciton Interaction and Optical Gain in Colloidal CdSe/CdS Dot/Rod Nanocrystals. *Adv. Mater.* **2009**, *21*, 4942–4946.

(24) Carbone, L.; Nobile, C.; De Giorgi, M.; Sala, F. D.; Morello, G.; Pompa, P.; Hych, P.; Snoeck, E.; Fiore, A.; Franchini, I. R.; et al. Synthesis and Micrometer-Scale Assembly of Colloidal CdSe/CdS Nanorods Prepared by a Seeded Growth Approach. *Nano Lett.* **2007**, *7*, 2942–2950.

(25) Deka, S.; Quarta, A.; Lupo, M. G.; Falqui, A.; Boninelli, S.; Giannini, C.; Morello, G.; De Giorgi, M.; Lanzani, G.; Spinella, C.; et al. CdSe/ZnS Double Shell Nanorods with High Photoluminescence Efficiency and Their Exploitation as Biolabeling Probes. *J. Am. Chem. Soc.* **2009**, *131*, 2948–2958.

(26) Lupo, M. G.; Della Sala, F.; Carbone, L.; Zavelani-Rossi, M.; Fiore, A.; Luer, L.; Polli, D.; Cingolani, R.; Manna, L.; Lanzani, G.

Ultrafast Electron-Hole Dynamics in Core/Shell CdSe/CdS Dot/Rod Nanocrystals. *Nano Lett.* **2008**, *8*, 4582–4587.

(27) Luo, Y.; Wang, L. W. Electronic Structures of the CdSe/CdS Core–Shell Nanorods. *ACS Nano* **2010**, *4*, 91–98.

(28) Borys, N. J.; Walter, M. J.; Huang, J.; Talapin, D. V.; Lupton, J. M. The Role of Particle Morphology in Interfacial Energy Transfer in CdSe/CdS Heterostructure Nanocrystals. *Science* **2010**, *330*, 1371–1374.

(29) Amirav, L.; Alivisatos, A. P. Photocatalytic Hydrogen Production with Tunable Nanorod Heterostructures. *J. Phys. Chem. Lett.* **2010**, *1*, 1051–1054.

(30) Yoskovitz, E.; Menagen, G.; Sitt, A.; Lachman, E.; Banin, U. Nanoscale Near-Field Imaging of Excitons in Single Heterostructured Nanorods. *Nano Lett.* **2010**, *10*, 3068–3072.

(31) The excitation wavelength for the QY measurement in ref 24 is not directly mentioned. It is presumably the same as that in ref 25.

(32) Bawendi, M. G.; Steigerwald, M. L.; Brus, L. E. The Quantum-Mechanics of Larger Semiconductor Clusters (Quantum Dots). *Annu. Rev. Phys. Chem.* **1990**, *41*, 477–496.

(33) Schooss, D.; Mews, A.; Eychmuller, A.; Weller, H. Quantum-Dot Quantum-Well CdS/HgS/CdS — Theory and Experiment. *Phys. Rev. B* **1994**, *49*, 17072–17078.

(34) Nozik, A. J. Spectroscopy and Hot Electron Relaxation Dynamics in Semiconductor Quantum Wells and Quantum Dots. *Annu. Rev. Phys. Chem.* **2001**, *52*, 193–231.

(35) Schroeter, D. F.; Griffiths, D. J.; Sercel, P. C. Defect-Assisted Relaxation in Quantum Dots at Low Temperature. *Phys. Rev. B* **1996**, *54*, 1486–1489.

(36) Sercel, P. C. Multiphonon-Assisted Tunneling through Deep Levels — A Rapid Energy-Relaxation Mechanism in Nonideal Quantum-Dot Heterostructures. *Phys. Rev. B* **1995**, *51*, 14532–14541.

(37) Pandey, A.; Guyot-Sionnest, P. Slow Electron Cooling in Colloidal Quantum Dots. *Science* **2008**, *322*, 929–932.

(38) Huang, J. E.; Huang, Z. Q.; Jin, S. Y.; Lian, T. Q. Exciton Dissociation in CdSe Quantum Dots by Hole Transfer to Phenothiazine. *J. Phys. Chem. C* **2008**, *112*, 19734–19738.

(39) Jin, S. Y.; Hsiang, J. C.; Zhu, H. M.; Song, N. H.; Dickson, R. M.; Lian, T. Q. Correlated Single Quantum Dot Blinking and Interfacial Electron Transfer Dynamics. *Chem. Sci.* **2010**, *1*, 519–526.

(40) Sharma, S. N.; Pillai, Z. S.; Kamat, P. V. Photoinduced Charge Transfer between CdSe Quantum Dots and *p*-Phenylenediamine. *J. Phys. Chem. B* **2003**, *107*, 10088–10093.

(41) Chen, Y.; Vela, J.; Htoon, H.; Casson, J. L.; Werder, D. J.; Bussian, D. A.; Klimov, V. I.; Hollingsworth, J. A. "Giant" Multishell CdSe Nanocrystal Quantum Dots with Suppressed Blinking. *J. Am. Chem. Soc.* **2008**, *130*, 5026–5027.

(42) Mahler, B.; Spinicelli, P.; Buil, S.; Quelin, X.; Hermier, J. P.; Dubret, B. Towards Non-Blinking Colloidal Quantum Dots. *Nat. Mater.* **2008**, *7*, 659–664.

(43) Garcia-Santamaria, F.; Brovelli, S.; Viswanatha, R.; Hollingsworth, J. A.; Htoon, H.; Crooker, S. A.; Klimov, V. I. Breakdown of Volume Scaling in Auger Recombination in CdSe/CdS Heteronanocrystals: The Role of the Core-Shell Interface. *Nano Lett.* **2011**, *11*, 687–693.

(44) Fisher, B. R.; Eisler, H. J.; Stott, N. E.; Bawendi, M. G. Emission Intensity Dependence and Single-Exponential Behavior in Single Colloidal Quantum Dot Fluorescence Lifetimes. *J. Phys. Chem. B* **2004**, *108*, 143–148.

(45) See, for example: Atkins, P.; de Paula, J. *Physical Chemistry*, 7th ed.; W. H. Freeman: New York, 2001; p 927.

(46) Piryatinski, A.; Ivanov, S. A.; Tretiak, S.; Klimov, V. I. Effect of Quantum and Dielectric Confinement on the Exciton–Exciton Interaction Energy in Type II Core/Shell Semiconductor Nanocrystals. *Nano Lett.* **2007**, *7*, 108–115.

(47) Aharoni, A.; Mokari, T.; Popov, I.; Banin, U. Synthesis of InAs/CdSe/ZnSe Core/Shell1/Shell2 Structures with Bright and Stable near-Infrared Fluorescence. *J. Am. Chem. Soc.* **2006**, *128*, 257–264.

(48) Chen, X. B.; Lou, Y. B.; Samia, A. C.; Burda, C. Coherency Strain Effects on the Optical Response of Core/Shell Heteronanostructures. *Nano Lett.* **2003**, *3*, 799–803.

(49) Choi, C. L.; Koski, K. J.; Sivasankar, S.; Alivisatos, A. P. Strain-Dependent Photoluminescence Behavior of CdSe/CdS Nanocrystals with Spherical, Linear, and Branched Topologies. *Nano Lett.* **2009**, *9*, 3544–3549.

(50) Klimov, V. I. Optical Nonlinearities and Ultrafast Carrier Dynamics in Semiconductor Nanocrystals. *J. Phys. Chem. B* **2000**, *104*, 6112–6123.

(51) Klimov, V. I. Spectral and Dynamical Properties of Multi-excitons in Semiconductor Nanocrystals. *Annu. Rev. Phys. Chem.* **2007**, *58*, 635–673.

(52) Hunsche, S.; Dekorsy, T.; Klimov, V.; Kurz, H. Ultrafast Dynamics of Carrier-Induced Absorption Changes in Highly-Excited Cdse Nanocrystals. *Appl. Phys. B: Laser Opt.* **1996**, *62*, 3–10.

(53) Hewa-Kasakarage, N. N.; El-Khoury, P. Z.; Tarnovsky, A. N.; Kirsanova, M.; Nemitz, I.; Nemchinov, A.; Zamkov, M. Ultrafast Carrier Dynamics in Type II ZnSe/CdS/ZnSe Nanobarbells. *ACS Nano* **2010**, *4*, 1837–1844.

(54) Rain, G.; Stferle, T.; Moreels, I.; Gomes, R.; Kamal, J. S.; Hens, Z.; Mahrt, R. F. Probing the Wave Function Delocalization in CdSe/CdS Dot-in-Rod Nanocrystals by Time- and Temperature-Resolved Spectroscopy. *ACS Nano* **2011** 10.1021/nn2005969.